

On the time dependency of a_0

Antonino Del Popolo^{1,2,3,*} and Man Ho Chan⁴

¹*Dipartimento di Fisica e Astronomia, University of Catania, Viale Andrea Doria 6, 95125 Catania, Italy*

²*Institute of Astronomy, Russian Academy of Sciences, Pyatnitskaya str. 48, 119017 Moscow, Russia*

³*Institute of Astronomy and National Astronomical Observatory,*

Bulgarian Academy of Sciences, 72 Tsarigradsko Shosse Blvd., 1784 Sofia, Bulgaria

⁴*Department of Science and Environmental Studies, The Education University of Hong Kong, Tai Po, New Territories, Hong Kong, China*

(Dated: May 6, 2024)

In this paper, we test one of the predictions of the Scale Invariant Vacuum (SIV) theory on MOND. According to that theory, MOND's acceleration a_0 is not a universal quantity but depends on several parameters, including time. To check this prediction, we compare the dependency of a_0 from redshift, using the values of a_0 obtained in Marra *et al.* [1] by carrying a Bayesian inference for 153 galaxies of the SPARC sample. Since this sample does not contain galaxies at large redshift, we have estimated a_0 from the data in Nestor Shachar *et al.* [2]. The SPARC sample, for small values of the redshift, in the redshift range $0.00032 - 0.032$ gives a correlation with z , while the Nestor Shachar *et al.* [2] data, in the higher redshift range $0.5 - 2.5$ gives an anti-correlation with the redshift z . Both samples show a dependency of a_0 from z , although the uncertainties involved are large, especially for the high-redshift galaxies. The combined sample gives an overall correlation of a_0 with z . The different behavior at low and high redshift can be related to a change of the $a_0(z)$ with redshift, or to the lower precision with which the high-redshift value of a_0 are known.

PACS numbers: 98.52.Wz, 98.65.Cw

Keywords: Dwarf galaxies; galaxy clusters; modified gravity; mass-temperature relation

I. INTRODUCTION

In the past decades, the Λ CDM model showed to be a very good model in predicting observations on cosmological scales [3–5], except some drawbacks, and on intermediate scales ([5–10]). Some of the drawbacks on cosmological scales are the cosmic coincidence problem [11], the cosmological constant problem [12, 13], the Hubble tension, namely a discrepancy in H_0 , the current value of the Hubble parameter, in which the value fitted using the CMB is different from that in the local universe using supernovae and stars [14]. The CMB also shows an unexpected cold spot [15–17], a quadrupole-octupole alignment [18–22], a hemispherical asymmetry [23–28], and another tension concerning the growth rate of perturbations, σ_8 , when using different measurements [29, 30]. Another problem of the model is that the constituents of dark matter have never been detected, and there are no clues on what “dark energy” could be. In the scale $1 - 10$ kpcs, the Λ CDM model suffers from the so called “small scale problems, like the “Cusp/Core” problem [31–36][37–42] the “missing satellite problem” [43, 44], etc. Apart drastic solutions to solve the “small scale problems”, like modifying the particles constituting dark matter ([45–48]), or modifying the power spectrum (e.g. [49]), astrophysical solutions have been proposed based on the role of baryons ([36, 38, 39, 50–59]). Another solution proposed to solve some of the drawbacks of the Λ CDM model is modifying the theory of gravity ([60–64]). In some cases these theories do not even need dark matter and dark energy, like for example the MOND theory [65]. Another theory without the need of the two quoted components is the Scale Invariant Vacuum (SIV) theory, based on

the hypothesis that the macroscopic space is scale invariant.

In [66], the relations between SIV and MOND were studied. The author found the deep-MOND limit equations are re-obtained, and that contrarily to MOND assumption, a_0 is not a universal constant but is time dependent. In the present paper, we want to check the time dependency prediction of a_0 . For this aim, we will use the SPARC sample and Nestor Shachar *et al.* [2] data, to calculate the values of a_0 and their relation with the redshift z . The paper is organized as follows. Section II describes SIV, and its connection with MOND. In Section III, we discuss the data and statistical analysis. Section IV and V are devoted to discussion and conclusion, respectively.

II. a_0 TIME DEPENDENCE

One of the central point in MOND is the existence of an universal acceleration, namely a_0 , that distinguishes between the Newtonian and non-Newtonian behavior of a system. Nevertheless MOND theory claims that a_0 is universal and constant with a value $a_0 = 1.2 \times 10^{-8}$ cm/s². Several studies have shown that this is not the case [1, 59, 67–71]. However, none of the previous studies has considered the possibility that a_0 is time-dependent. Based on the claims in [66, 72] that a_0 should be a time-dependent quantity, and the relation between SIV and MOND theories (see the Appendix), in this paper, we would like to check this possibility.

III. DATA AND STATISTICAL ANALYSIS

As mentioned above, in the paper, we use the SPARC (*Spitzer* Photometry and Accurate Rotation Curves) dataset [73] for analysis. The dataset is constituted by 175 late-type

* antonino.delpopolo@unict.it

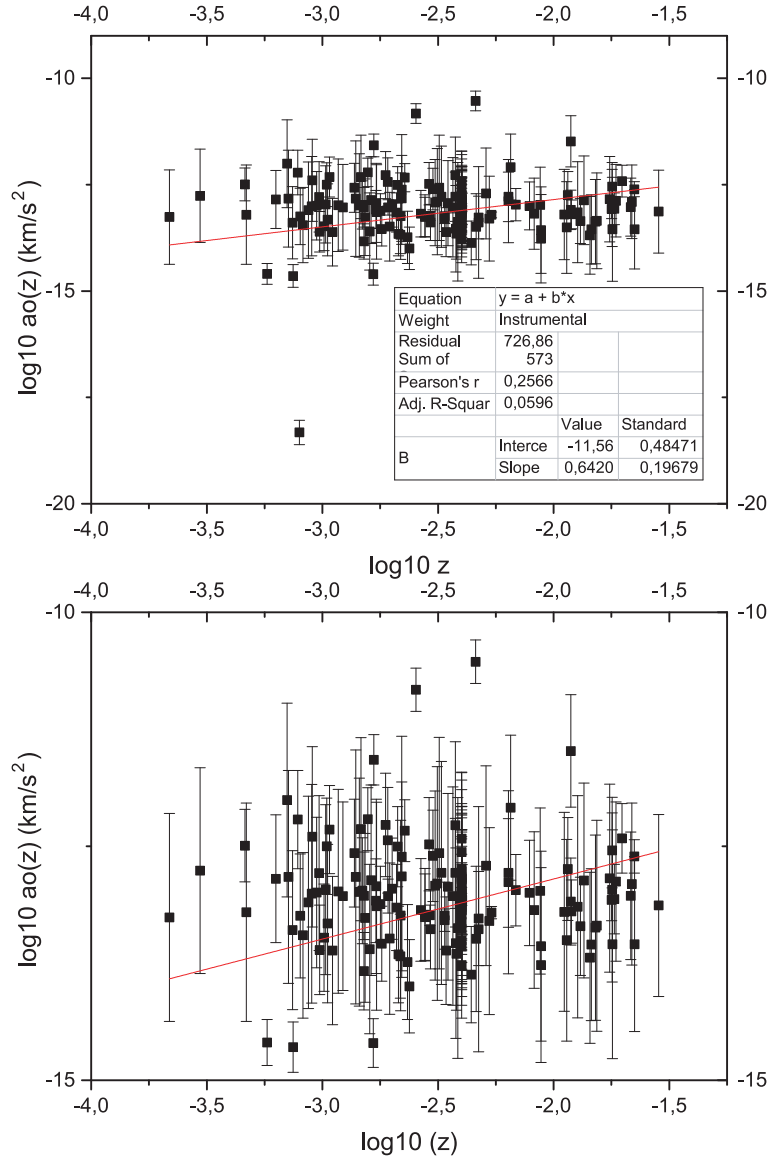


FIG. 1. Upper panel: The black dots with error bars represent the values of a_0 (with 1σ standard deviation) against redshift z obtained from the SPARC data. The red solid line indicates the non-linear fit to the data points. Bottom panel: same as the top panel but with a different ordinate axis scale.

galaxies with surface photometry at $3.6 \mu\text{m}$, and with high quality rotation curves obtained from HI/H α studies. The gas mass is provided by 21 cm observations. The morphologies present in SPARC span from S0 to Irr. Almost all SPARC galaxies have a disc structure, with some having also bulges. The baryon component is constituted by the disc, bulge, and gas components. The SPARC dataset, with some quality cuts, was used by [74] to derive the radial acceleration relation (RAR), and by [1] to perform a test on MOND, based on [67–69]. After the quoted cuts described in [1, 74], 153 galaxies are left. [1] carried a Bayesian inference for the quoted 153 galaxies. They adopted for each galaxy the Gaussian likelihood

$$\mathcal{L}(\theta) = |2\pi\Sigma|^{-1/2} e^{-\chi^2(\theta)/2}, \quad (1)$$

where Σ is the covariance matrix described in [1], and $\chi^2 = \chi^2(A_0, Y_b, Y_d, D, I)$, with

$$\chi^2 = \sum_{i=1}^N \left(\frac{V_M(R_i, A_0, Y_b, Y_d, D) - V_{C,i} \frac{\sin I_0}{\sin I}}{\sigma_{V,i} \frac{\sin I_0}{\sin I}} \right)^2. \quad (2)$$

In Eq. (2), N is the number of data points relative to the given galaxy data, V_M is the circular velocity of the model, R_i represents the galaxy radius at which the circular velocity $V_{C,i}$ was measured, $\sigma_{V,i}$ is the corresponding error, and I_0 is the inclination, given together with $V_{C,i}$ and $\sigma_{V,i}$ by SPARC. The model velocity V_M is obtained from MOND using the interpolating function

$$\mathbf{a} = \frac{\mathbf{aN}}{1 - e^{-\sqrt{a_n/a_0}}} \quad (3)$$

the Newtonian velocity, V_N ,

$$V_N^2 = \Upsilon_b |V_b| V_b + \Upsilon_d |V_d| V_d + |V_{\text{gas}}| V_{\text{gas}}. \quad (4)$$

Here, the subscripts b and d stand for bulge and disc respectively, and Υ_b and Υ_d are the corresponding mass-to-light ratios, with the distance correction given in Eq. 5 of [1]. The priors chosen, the quality cuts, and the determination of the global best value are described in Sections 4.2, 4.3, and 4.4 of [1] respectively.

Moreover, based on the data of the high-redshift galaxies in Nestor Shachar *et al.* [2], we can get a sample of high-redshift galaxies for analysis. These samples can represent the average values of a_0 at high redshift ($z = 0.5 - 2.5$). However, it is very difficult to obtain the value of a_0 for each of these high-redshift galaxies because the data of the galactic rotation curve profiles are too few. Fortunately, there are some galaxies in which the gravitational acceleration at the effective radius R_e is smaller than the characteristic acceleration scale a_0 . That means the position at R_e for these galaxies are approximately located at the deep-MOND regime. In this regime, we have [75]

$$V_c^4 = GM_B a_0, \quad (5)$$

where V_c is the rotation velocity at R_e and M_B is the total baryonic mass within R_e . From Table 3 of Nestor Shachar *et al.* [2], we find that there are 17 galaxies in which the gravitational acceleration is smaller than the typical $a_0 = 1.2 \times 10^{-8} \text{ cm/s}^2$ at R_e . We plot the values of a_0 as a function of z in Fig. 2. We can see a very small decreasing trend exists in the plot when z is larger. Unfortunately, the uncertainties of the high-redshift rotation curve data are very large. Therefore, the result here can be used as a reference only.

IV. DISCUSSION

The MOND paradigm is successful in describing rotation curves, and other astrophysical aspects. It is based on the idea that Newtonian mechanics is valid only for higher values of gravitational acceleration, and for lower values it must be modified. The threshold between the regimes in which Newtonian mechanics, and MOND are to be applied is related to an universal parameter of the model, the acceleration a_0 . Several studies have shown that in reality a_0 is not a universal constant [59, 67–71] depending on several parameters. Prompted by the paper of [66], showing that the SIV theory reduces to MOND prediction of the acceleration, in certain limits, and that the acceleration a_0 of MOND cannot be a universal constant but a parameter that changes with time, we checked this possibility. Using the values of a_0 , and their errors obtained by [1], which are an improvement on that obtained in [67] using Bayesian statistics, and the redshift of the same galaxies, we studied the case of a_0 being a function of redshift. Then, we performed a non-linear fitting using the Levenberg-Marquardt algorithm, on the [1] data, in order to account for errors in the dependent variable. The result is shown in Fig. 1. the top and bottom panel represent the same fit considering

different scale for the box. The plot clearly shows a correlation between a_0 , and redshift. The Pearson's r coefficient is 0.25661. The other estimated parameters of the fit are written directly on the Fig. 1. It is interesting to note that the redshift range is 0.00032-0.032, namely even for low redshift the correlation is present. In order to see if the correlation continues to persist going towards larger redshifts, we used the data of the high-redshift galaxies in Nestor Shachar *et al.* [2]. These samples have much larger redshift than SPARC, with redshift in the range $z = 0.5 - 2.5$. While in the case of the SPARC sample the values of a_0 were obtained from the rotation curves using solid statistical methods, in the case of Nestor Shachar *et al.* [2] sample, we do not have the rotation curves of the galaxies, and we cannot obtain a_0 with the methods applied to the SPARC sample. Since the gravitational acceleration at the effective radius R_e , for some galaxies, is smaller than a_0 , and they are located in the deep-MOND regime, and in this case we can get an approximate value of a_0 from the relation $V_c^4 = GM_B a_0$, where M_B is the total baryonic mass within R_e , and V_c is the rotation velocity at R_e . Clearly this is just an estimate that cannot be precise as the a_0 obtained from SPARC with Bayesian statistics. We used 17 galaxies from Nestor Shachar *et al.* [2], those having the gravitational acceleration smaller than the typical $a_0 = 1.2 \times 10^{-8} \text{ cm/s}^2$ at R_e . Then, we fitted with the same method used for the SPARC galaxies (Fig. 1), the a_0 s estimated from Nestor Shachar *et al.* [2] data. The result is shown in Fig. 2. The fit shows a anti-correlation between a_0 and the redshift weaker than in the case of the SPARC sample. The Pearson's r coefficient is in this case -0.116, and the other parameters of the fit are written on Fig. 2. As reported, Fig. 2 shows an anti-correlation of a_0 with z , while Fig. 1 a correlation between the same quantities. The reason leading to this could be several. As Fig. 2 shows, the error bars in a_0 are very large, and the fitting algorithm is sensitive to the errors. Small changes in the errors could produce a different behavior on the fit.

Note that the values of a_0 obtained in Fig. 1 and in Fig. 2 are following different methods. Generally speaking, using Bayesian method to get the values of a_0 would be more reliable. However, for the high-redshift galaxies, the data points of the rotation curves are too few. The number of variables involved in the Bayesian analysis would be larger than or almost the same as the number of data points. In this situation, the results from the Bayesian analysis would not be reliable. Therefore, we need to use another method (i.e. the deep-MOND regime approximation) to get the values of a_0 . Although the methods used in the two samples are different, the values of a_0 found in the two different samples originate from the same MOND framework. Nevertheless, the values of a_0 obtained for the high-redshift galaxies are not known with the precision of those of SPARC, and probably the result in Fig. 2 is less reliable than that in Fig. 1. A last possibility is that the a_0 dependence on redshift is non-linear: it increases reaches a maximum and then decreases. In order to evaluate these possibilities, it would be necessary to find other galaxies at high redshift for which the rotation curves are known. In any case, we are more interested in the overall trend of a_0 with redshift. For this reason, we plotted all the data on the same plot in Fig.

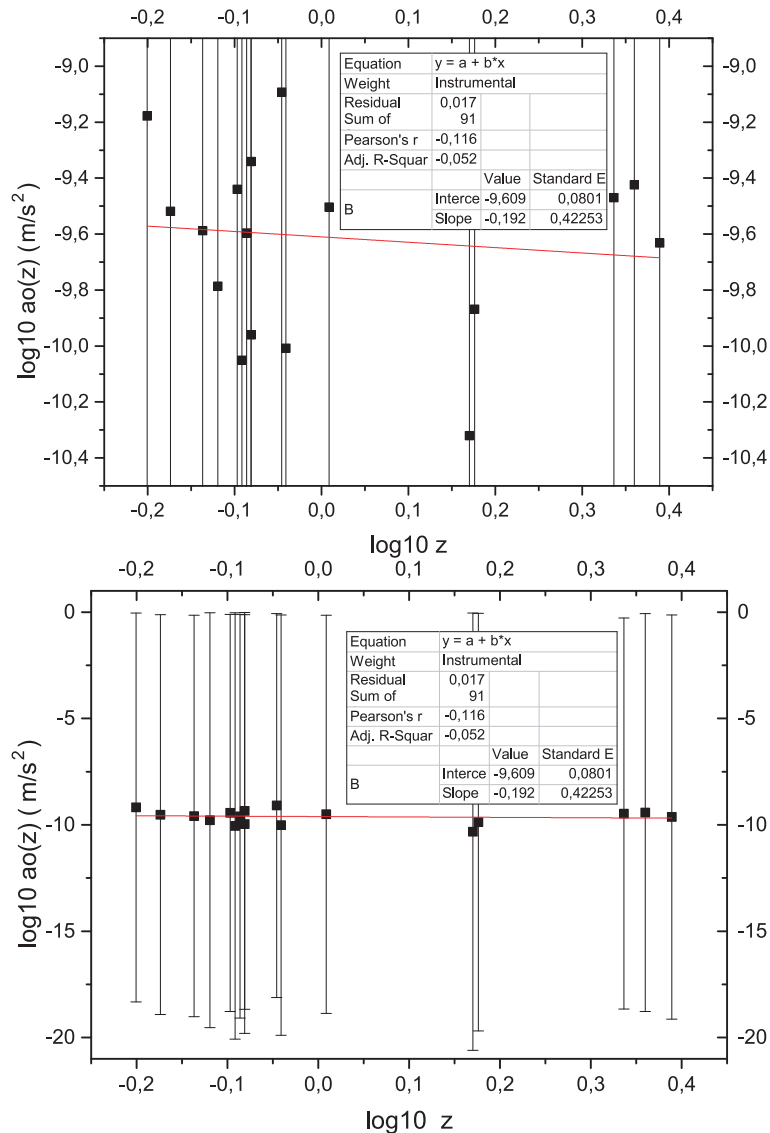


FIG. 2. Top panel: The black dots with error bars represent the values of a_0 (with 1σ standard deviation) against redshift z obtained from the Nestor Shachar *et al.* [2] data. The red solid line indicates the non-linear fit to the data points. Bottom panel: same as the top panel but with a different ordinate axis scale.

3, and fitted again the data. The final result is that there is a correlation between a_0 , and redshift. The Pearson's r coefficient is 0.26. Apart from the results using galaxies, some previous studies using the data of galaxy clusters (HIFLUGCS and CLASH samples) have obtained larger values of a_0 by analysing the radial acceleration relation [76, 77]. The redshift ranges of the data samples HIFLUGCS and CLASH are $z \sim 0.01-0.2$ and $z \sim 0.2-0.7$ respectively, which are in between the SPARC sample and the high-redshift galaxies used in this study. The values of a_0 obtained are $a_0 \sim 10^{-7} \text{ cm/s}^2$, which are larger than that shown in galaxies. Therefore, these

show that the value of a_0 might not be a constant. We anticipate that more data ranging from galaxies to galaxy clusters with different redshifts can further verify our proposal.

V. CONCLUSION

According to the Λ CDM model, universe is dominated by dark matter, and dark energy. Nevertheless, this dark matter component remains undetected from many different experiments. Concerning dark energy, the situation is even worse

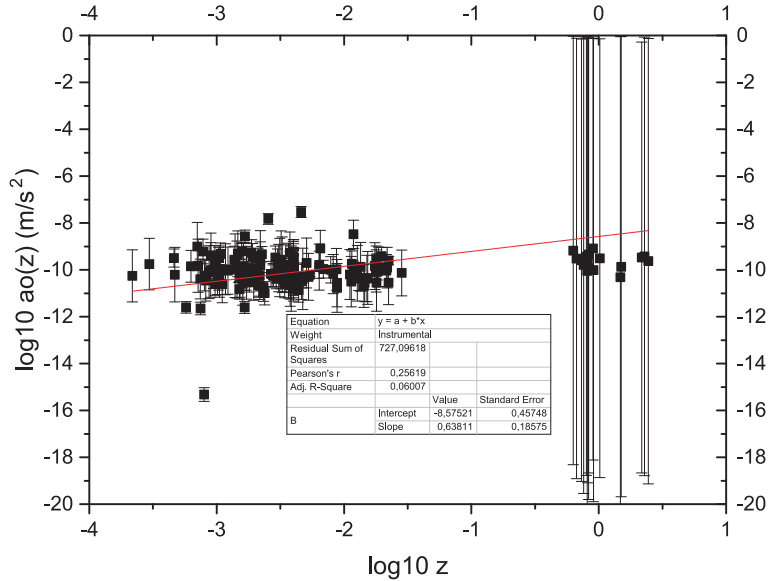


FIG. 3. The black dots with error bars represent the values of a_0 (with 1σ standard deviation) against redshift z obtained from all the data we have. The red solid line indicates the non-linear fit to the data points.

since we do not really know what dark energy is composed of. Moreover, the Λ CDM model shows some drawbacks especially at small scales. In order to solve those drawbacks in the Λ CDM model, several authors have proposed to modify the theory of gravity ([60–64]). In some of these modified gravity theories, dark matter and dark energy are not needed. One of these theories is the Scale Invariant Vacuum (SIV) theory, based on the hypothesis that the macroscopic space is scale invariant. One of the predictions of this theory is that the quantity a_0 in MOND is time-dependent. In order to check this prediction, we compared the dependency of a_0 from redshift, using two groups of data. The first one, of higher quality, and low values of z , is obtained in Marra *et al.* [1] by carrying a Bayesian inference for 153 galaxies of the SPARC sample. The second one, of lower quality but larger redshift is obtained from the data in Nestor Shachar *et al.* [2]. Both sample shows a dependency a_0 from redshift, although the involved uncertainties are large, especially for the high-redshift galaxies. The a_0 obtained from the SPARC sample shows a correlation with z , at small redshifts, while the a_0 obtained from the data of Nestor Shachar *et al.* [2] shows an anti-correlation with redshift, at higher z . In other terms, both samples show a dependency of a_0 from redshift. The difference of behavior at small and larger redshift can be due to a change of the behavior of a_0 with z , or to the lower quality of the high redshift data. The combined data give a correlation of a_0 with z .

APPENDIX

Scale invariance was considered by Weyl, and Eddington [78] in order to account for gravitation, and electromagnetism by the space-time geometry. It was initially abandoned because particle properties were dependent on its past worldline. Considering the Weyl Integrable Geometry (WIG), the problem is solved [79, 80]. By scale invariance one means that through a transformation of the line element like

$$ds' = \lambda(x^\mu) ds, \quad (6)$$

the basic equations do not change. $\lambda(x^\mu)$ is the scale factor, ds' refers to general relativity (GR), while ds refers to the WIG space. [81] studied the WIG geometrical properties, and geodesics, while [82] studied the weak field limit. Differently from GR is present a small additional acceleration in the direction of motion. Several studies, with positive results, have been performed on the rotation of galaxies, the dynamics of clusters of galaxies, on the growth of density fluctuation in the early universe, on inflation, on lunar recession (see [66, 72] for the references).

In [66, 72], the SIV basic theoretical context, and the cosmological solutions are given. We are interested in the weak field approximation, and the MOND approximation. The weak field approximation was obtained by [82], and can be expressed, in spherical coordinates, as

$$\frac{d^2 \mathbf{r}}{dt^2} = -\frac{G_t M(t)}{r^2} \frac{\mathbf{r}}{r} + \kappa(t) \frac{d\mathbf{r}}{dt}. \quad (7)$$

The extra term is called *the dynamical gravity*. This term, which is proportional to the velocity, favors outwards motion

during the expansion, and collapse during a contraction. In the case of a dust Universe, the conservation law imposes $\rho a^3 \lambda = \text{const.}$. This means that the inertial mass of a particle is not a constant, and moreover it depends on the factor λ . The time dependency of mass can be expressed as $M(t) = M(t_0)(t/t_0)$. In the case $\Omega_m = 0.3$, the mass at the Big-Bang was, $M(t_{\text{in}}) = \Omega_m^{1/3} M(t_0) = 0.6694 M(t_0)$, where is $t_0 = 1$ at present and $t_{\text{in}} = \Omega_m^{1/3}$ at the origin. The timescale τ in years is defined as $\tau_0 = 13.8$ Gyr, and $\tau_{\text{in}} = 0$ at the Big-Bang. τ , and t are related by

$$\frac{\tau - \tau_{\text{in}}}{\tau_0 - \tau_{\text{in}}} = \frac{t - t_{\text{in}}}{t_0 - t_{\text{in}}}, \quad (8)$$

and

$$\tau = \tau_0 \frac{t - \Omega_m^{1/3}}{1 - \Omega_m^{1/3}} \quad \text{and} \quad t = \Omega_m^{1/3} + \frac{\tau}{\tau_0}(1 - \Omega_m^{1/3}), \quad (9)$$

At present time, τ_0 , the modified Newton's equation is given by

$$\frac{d^2 \mathbf{r}}{d\tau^2} = -\frac{G M(\tau_0)}{r^2} \frac{\mathbf{r}}{r} + \frac{\psi_0}{\tau_0} \frac{d\mathbf{r}}{d\tau}. \quad (10)$$

where

$$G = G_t \left(\frac{dt}{d\tau} \right)^2 \quad (11)$$

and

$$\psi(\tau) = \frac{t_0 - t_{\text{in}}}{t_{\text{in}} + \frac{\tau}{\tau_0}(t_0 - t_{\text{in}})}; \quad \text{and} \quad \psi_0 = \psi(\tau_0) = 1 - \Omega_m^{1/3}. \quad (12)$$

In the case of galaxies, having rotation periods of some hundred years, λ , and M can be considered constant at the level of 1%. In Eq. (10) the dynamical gravity, namely the term proportional to κ disappears. Considering the transformations $r = \lambda r'$ and $t = \lambda t'$, and applying to the Newton equation expressed in the prime coordinates gives,

$$\frac{d^2 r'}{dt'^2} = -\frac{GM}{r'^2} \equiv g'_N. \quad (13)$$

In the system (r, t) the total acceleration g is,

$$g = \frac{d^2 r}{dt^2} = \frac{1}{\lambda} \frac{d^2 r'}{dt'^2}. \quad (14)$$

The accelerations g_N and g'_N are related by,

$$g_N \equiv -\frac{GM}{r^2} = -\frac{1}{\lambda^2} \frac{GM}{r'^2} \equiv \frac{1}{\lambda^2} g'_N. \quad (15)$$

Then the total acceleration is

$$g = \frac{d^2 r}{dt^2} = \frac{1}{\lambda} \frac{d^2 r'}{dt'^2} = \frac{1}{\lambda} g'_N = \lambda g_N, \quad (16)$$

and finally

$$g = \frac{d^2 r}{dt^2} = \lambda g_N = \left(\frac{g'_N}{g_N} \right)^{1/2} g_N = (g'_N g_N)^{1/2}. \quad (17)$$

In the deep-MOND regime limit we have

$$g = \sqrt{a_0 g_N} \quad (18)$$

and then comparing, $g'_N = a_0$. So, in the initial approximation of constant λ , and M , the scale invariant theory leads us to the deep-MOND limit, and moreover a_0 is time dependent like λ (in the general case). Another way to obtain the MOND behavior from Eq. (10) is to consider low gravities. In this case, one can show that

$$g = g_N \left[1 + \frac{\sqrt{2} \psi_0}{\xi} \left(\frac{g_c}{g_N} \right)^{1/2} \right]. \quad (19)$$

where g_c is the mean gravity at the edge of a sphere having the critical density, $\xi = \tau_0 H_0$, and ψ_0 depends on Ω_m (see Eq. (21)). For regions at large distances from the galactic center the previous equation reduces to

$$g \simeq \frac{\sqrt{2} \psi_0}{\xi} (g_c g_N)^{1/2} \quad (20)$$

where

$$\frac{\sqrt{2} \psi_0}{\xi} = \frac{\sqrt{2} (1 - \Omega_m^{1/3})}{H(\tau_0) \tau_0} = \frac{(1 - \Omega_m)}{\sqrt{2}}, \quad (21)$$

So, in the weak field limit, Eq. (10) leads to Eq. (20) which is equivalent to the deep-MOND limit, namely Eq. (18).

In the case of SIV or Λ CDM models with Ω_m in the range 0.2 – 0.3, we have

$$a_0 = \frac{(1 - \Omega_m)^2}{4} n c H_0 \quad (22)$$

or

$$a_0 = \frac{n c (1 - \Omega_m) (1 - \Omega_m^{1/3})}{2 \tau_0} \quad (23)$$

n depends on the cosmology, and is defined in [66].

Summarizing, according to SIV, a_0 is not a universal constant, but depends on time, H_0 , and Ω_m .

[1] V. Marra, D. C. Rodrigues, and Á. O. F. de Almeida, *MNRAS* **494**, 2875 (2020), arXiv:2002.03946 [astro-ph.GA].

[2] A. Nestor Shachar, S. H. Price, N. M. Förster Schreiber, R. Genzel, T. T. Shimizu, L. J. Tacconi, H. Übler, A. Burkert,

- R. I. Davies, A. Dekel, R. Herrera-Camus, L. L. Lee, D. Liu, D. Lutz, T. Naab, R. Neri, A. Renzini, R. Saglia, K. F. Schuster, A. Sternberg, E. Wisnioski, and S. Wuyts, *ApJ* **944**, 78 (2023), [arXiv:2209.12199 \[astro-ph.GA\]](#).
- [3] E. Komatsu, K. M. Smith, J. Dunkley, C. L. Bennett, B. Gold, G. Hinshaw, N. Jarosik, D. Larson, M. R. Nolta, and L. Page, *ApJS* **192**, 18 (2011), [arXiv:1001.4538 \[astro-ph.CO\]](#).
- [4] A. Del Popolo, *Astronomy Reports* **51**, 169 (2007), [arXiv:0801.1091 \[astro-ph\]](#).
- [5] A. Del Popolo, *American Institute of Physics Conference Series*, *American Institute of Physics Conference Series*, **1548**, 2 (2013).
- [6] D. N. Spergel, L. Verde, H. V. Peiris, E. Komatsu, M. R. Nolta, C. L. Bennett, M. Halpern, G. Hinshaw, N. Jarosik, A. Kogut, M. Limon, S. S. Meyer, L. Page, G. S. Tucker, J. L. Weiland, E. Wollack, and E. L. Wright, *ApJS* **148**, 175 (2003), [astro-ph/0302209](#).
- [7] M. Kowalski, D. Rubin, G. Aldering, R. J. Agostinho, A. Amadon, R. Amanullah, C. Balland, K. Barbary, G. Blanc, P. J. Challis, A. Conley, and e. a. Connolly, N. V., *ApJ* **686**, 749 (2008), [arXiv:0804.4142](#).
- [8] W. J. Percival, B. A. Reid, D. J. Eisenstein, N. A. Bahcall, T. Budavari, J. A. Frieman, M. Fukugita, J. E. Gunn, and e. a. Ivezić, *MNRAS* **401**, 2148 (2010), [arXiv:0907.1660 \[astro-ph.CO\]](#).
- [9] E. Komatsu, K. M. Smith, J. Dunkley, C. L. Bennett, B. Gold, G. Hinshaw, N. Jarosik, D. Larson, M. R. Nolta, and L. e. a. Page, *ApJS* **192**, 18 (2011), [arXiv:1001.4538 \[astro-ph.CO\]](#).
- [10] A. Del Popolo, *International Journal of Modern Physics D* **23**, 1430003 (2014), [arXiv:1305.0456 \[astro-ph.CO\]](#).
- [11] H. E. S. Velten, R. F. vom Martens, and W. Zimdahl, *European Physical Journal C* **74**, 3160 (2014), [arXiv:1410.2509 \[astro-ph.CO\]](#).
- [12] S. Weinberg, *Reviews of Modern Physics* **61**, 1 (1989).
- [13] A. V. Astashenok and A. del Popolo, *Classical and Quantum Gravity* **29**, 085014 (2012), [arXiv:1203.2290 \[gr-qc\]](#).
- [14] E. Di Valentino, O. Mena, S. Pan, L. Visinelli, W. Yang, A. Melchiorri, D. F. Mota, A. G. Riess, and J. Silk, *Classical and Quantum Gravity* **38**, 153001 (2021), [arXiv:2103.01183 \[astro-ph.CO\]](#).
- [15] M. Cruz, E. Martínez-González, P. Vielva, and L. Cayón, *MNRAS* **356**, 29 (2005), [astro-ph/0405341](#).
- [16] M. Cruz, M. Tucci, E. Martínez-González, and P. Vielva, *MNRAS* **369**, 57 (2006), [astro-ph/0601427](#).
- [17] M. Cruz, L. Cayón, E. Martínez-González, P. Vielva, and J. Jin, *ApJ* **655**, 11 (2007), [astro-ph/0603859](#).
- [18] D. J. Schwarz, G. D. Starkman, D. Huterer, and C. J. Copi, *Physical Review Letters* **93**, 221301 (2004), [astro-ph/0403353](#).
- [19] C. J. Copi, D. Huterer, D. J. Schwarz, and G. D. Starkman, *MNRAS* **367**, 79 (2006), [astro-ph/0508047](#).
- [20] C. J. Copi, D. Huterer, D. J. Schwarz, and G. D. Starkman, *Phys. Rev. D* **75**, 023507 (2007), [astro-ph/0605135](#).
- [21] C. J. Copi, D. Huterer, D. J. Schwarz, and G. D. Starkman, *Advances in Astronomy* **2010**, 847541 (2010), [arXiv:1004.5602 \[astro-ph.CO\]](#).
- [22] C. J. Copi, D. Huterer, D. J. Schwarz, and G. D. Starkman, *MNRAS* **449**, 3458 (2015), [arXiv:1311.4562](#).
- [23] H. K. Eriksen, F. K. Hansen, A. J. Banday, K. M. Górski, and P. B. Lilje, *ApJ* **605**, 14 (2004), [astro-ph/0307507](#).
- [24] F. K. Hansen, A. J. Banday, and K. M. Górski, *MNRAS* **354**, 641 (2004), [astro-ph/0404206](#).
- [25] T. R. Jaffe, A. J. Banday, H. K. Eriksen, K. M. Górski, and F. K. Hansen, *ApJL* **629**, L1 (2005), [astro-ph/0503213](#).
- [26] J. Hoftuft, H. K. Eriksen, A. J. Banday, K. M. Górski, F. K. Hansen, and P. B. Lilje, *ApJ* **699**, 985 (2009), [arXiv:0903.1229 \[astro-ph.CO\]](#).
- [27] Planck Collaboration, P. A. R. Ade, N. Aghanim, C. Armitage-Caplan, M. Arnaud, M. Ashdown, F. Atrio-Barandela, J. Aumont, C. Baccigalupi, A. J. Banday, and et al., *A&A* **571**, A23 (2014), [arXiv:1303.5083](#).
- [28] Y. Akrami, Y. Fantaye, A. Shafieloo, H. K. Eriksen, F. K. Hansen, A. J. Banday, and K. M. Górski, *ApJL* **784**, L42 (2014), [arXiv:1402.0870](#).
- [29] E. Macaulay, I. K. Wehus, and H. K. Eriksen, *Physical Review Letters* **111**, 161301 (2013), [arXiv:1303.6583](#).
- [30] M. Raveri, ArXiv e-prints (2015), [arXiv:1510.00688](#).
- [31] B. Moore, *Nature (London)* **370**, 629 (1994).
- [32] R. A. Flores and J. R. Primack, *ApJL* **427**, L1 (1994), [astro-ph/9402004](#).
- [33] A. Burkert, *ApJL* **447**, L25 (1995), [astro-ph/9504041](#).
- [34] W. J. G. de Blok, A. Bosma, and S. McGaugh, *MNRAS* **340**, 657 (2003), [astro-ph/0212102](#).
- [35] R. A. Swaters, B. F. Madore, F. C. van den Bosch, and M. Balcells, *ApJ* **583**, 732 (2003), [astro-ph/0210152](#).
- [36] A. Del Popolo, *ApJ* **698**, 2093 (2009), [arXiv:0906.4447 \[astro-ph.CO\]](#).
- [37] A. Del Popolo and P. Kroupa, *A&A* **502**, 733 (2009), [arXiv:0906.1146 \[astro-ph.CO\]](#).
- [38] A. Del Popolo, *MNRAS* **419**, 971 (2012), [arXiv:1105.0090 \[astro-ph.CO\]](#).
- [39] A. Del Popolo and N. Hiotelis, *JCAP* **1**, 047 (2014), [arXiv:1401.6577 \[astro-ph.GA\]](#).
- [40] J. F. Navarro, C. S. Frenk, and S. D. M. White, *ApJ* **462**, 563 (1996), [astro-ph/9508025](#).
- [41] J. F. Navarro, C. S. Frenk, and S. D. M. White, *ApJ* **490**, 493 (1997), [astro-ph/9611107](#).
- [42] J. F. Navarro, A. Ludlow, V. Springel, J. Wang, M. Vogelsberger, S. D. M. White, A. Jenkins, C. S. Frenk, and A. Helmi, *MNRAS* **402**, 21 (2010), [arXiv:0810.1522](#).
- [43] A. Klypin, A. V. Kravtsov, O. Valenzuela, and F. Prada, *ApJ* **522**, 82 (1999), [astro-ph/9901240](#).
- [44] B. Moore, T. Quinn, F. Governato, J. Stadel, and G. Lake, *MNRAS* **310**, 1147 (1999), [astro-ph/9903164](#).
- [45] P. Colín, V. Avila-Reese, and O. Valenzuela, *ApJ* **542**, 622 (2000), [astro-ph/0004115](#).
- [46] J. Sommer-Larsen and A. Dolgov, *ApJ* **551**, 608 (2001), [astro-ph/9912166](#).
- [47] J. Goodman, *New Astronomy* **5**, 103 (2000), [astro-ph/0003018](#).
- [48] P. J. E. Peebles, *ApJL* **534**, L127 (2000), [astro-ph/0002495](#).
- [49] A. R. Zentner and J. S. Bullock, *ApJ* **598**, 49 (2003), [astro-ph/0304292](#).
- [50] J. F. Navarro, V. R. Eke, and C. S. Frenk, *MNRAS* **283**, L72 (1996), [astro-ph/9610187](#).
- [51] S. Gelato and J. Sommer-Larsen, *MNRAS* **303**, 321 (1999), [astro-ph/9806289](#).
- [52] J. I. Read and G. Gilmore, *MNRAS* **356**, 107 (2005), [astro-ph/0409565](#).
- [53] S. Mashchenko, H. M. P. Couchman, and J. Wadsley, *Nature (London)* **442**, 539 (2006), [astro-ph/0605672](#).
- [54] F. Governato, C. Brook, L. Mayer, A. Brooks, G. Rhee, J. Wadsley, P. Jonsson, B. Willman, G. Stinson, T. Quinn, and P. Madau, *Nature (London)* **463**, 203 (2010), [arXiv:0911.2237 \[astro-ph.CO\]](#).
- [55] A. El-Zant, I. Shlosman, and Y. Hoffman, *ApJ* **560**, 636 (2001), [astro-ph/0103386](#).

- [56] A. A. El-Zant, Y. Hoffman, J. Primack, F. Combes, and I. Shlosman, *ApJL* **607**, L75 (2004), [astro-ph/0309412](#).
- [57] E. Romano-Díaz, I. Shlosman, Y. Hoffman, and C. Heller, *ApJL* **685**, L105 (2008), [arXiv:0808.0195](#).
- [58] D. R. Cole, W. Dehnen, and M. I. Wilkinson, *MNRAS* **416**, 1118 (2011), [arXiv:1105.4050 \[astro-ph.CO\]](#).
- [59] A. Saburova and A. Del Popolo, *MNRAS* **445**, 3512 (2014), [arXiv:1410.3052 \[astro-ph.GA\]](#).
- [60] H. A. Buchdahl, *MNRAS* **150**, 1 (1970).
- [61] A. A. Starobinsky, *Physics Letters B* **91**, 99 (1980).
- [62] M. Milgrom, *ApJ* **270**, 365 (1983).
- [63] M. Milgrom, *ApJ* **270**, 371 (1983).
- [64] R. Ferraro, *American Institute of Physics Conference Series*, *American Institute of Physics Conference Series*, **1471**, 103 (2012), [arXiv:1204.6273 \[gr-qc\]](#).
- [65] M. Milgrom, *ApJ* **306**, 9 (1986).
- [66] A. Maeder, *MNRAS* **520**, 1447 (2023), [arXiv:2302.06206 \[gr-qc\]](#).
- [67] D. C. Rodrigues, V. Marra, A. del Popolo, and Z. Davari, *Nature Astronomy* **2**, 668 (2018), [arXiv:1806.06803 \[astro-ph.GA\]](#).
- [68] D. C. Rodrigues, V. Marra, A. Del Popolo, and Z. Davari, *Nature Astronomy* **2**, 927 (2018), [arXiv:1811.05882 \[astro-ph.GA\]](#).
- [69] D. C. Rodrigues, V. Marra, A. Del Popolo, and Z. Davari, *Nature Astronomy* **4**, 134 (2020), [arXiv:2002.01970 \[astro-ph.GA\]](#).
- [70] Y. Zhou, A. Del Popolo, and Z. Chang, *Physics of the Dark Universe* **28**, 100468 (2020), [arXiv:2008.04065 \[astro-ph.GA\]](#).
- [71] A. Del Popolo, *Physics of the Dark Universe* **40**, 101203 (2023), [arXiv:2303.16658 \[astro-ph.CO\]](#).
- [72] A. Maeder and V. G. Gueorguiev, *Universe* **6**, 46 (2020).
- [73] F. Lelli, S. S. McGaugh, and J. M. Schombert, *Astron. J.* **152**, 157 (2016), [arXiv:1606.09251 \[astro-ph.GA\]](#).
- [74] S. S. McGaugh, F. Lelli, and J. M. Schombert, *Phys. Rev. Lett.* **117**, 201101 (2016), [arXiv:1609.05917 \[astro-ph.GA\]](#).
- [75] R. H. Sanders and S. S. McGaugh, *ARAA* **40**, 263 (2002), [arXiv:astro-ph/0204521 \[astro-ph\]](#).
- [76] M. H. Chan and A. Del Popolo, *MNRAS* **492**, 5865 (2020).
- [77] Y. Tian, K. Umetsu, C.-M. Ko, M. Donahue, and I.-N. Chiu, *ApJ* **896**, 70 (2020).
- [78] A. S. Eddington, *The mathematical theory of relativity* (1923).
- [79] P. A. M. Dirac, *Proceedings of the Royal Society of London Series A* **33**, 253 (1932).
- [80] V. Canuto, P. J. Adams, S. H. Hsieh, and E. Tsiang, *Phys. Rev. D* **16**, 1643 (1977).
- [81] P. Bouvier and A. Maeder, *Astrophysics and Space Science* **54**, 497 (1978).
- [82] A. Maeder and P. Bouvier, *A&A* **73**, 82 (1979).

TABLE I: (1) Galaxy name. (2) Best fit for $A_0 = \log_{10} a_0$ (km/s²). (3–8) A_0 credible intervals (1σ , 3σ , 5σ). (9–10) Distance (Mpc), Error. (11) $Z = \log_{10} z$.

Galaxy	A_0 best	$1\sigma_-$	$1\sigma_+$	$3\sigma_-$	$3\sigma_+$	$5\sigma_-$	$5\sigma_+$	D	D_{Error}	Z
CamB	-14.645	-0.614	0.462	-5.328	0.727	-5.328	1.287	3.36	0.26	-3.1237
D512-2	-13.241	-0.416	0.463	-1.388	1.963	-3.752	4.179	15.2	4.56	-2.4682
D564-8	-13.486	-0.147	0.164	-0.424	0.585	-0.71	1.212	8.79	0.28	-2.7061
D631-7	-13.14	-0.075	0.08	-0.214	0.259	-0.337	0.462	7.72	0.18	-2.7625
DDO064	-13.03	-0.317	0.363	-0.935	1.609	-1.679	2.535	6.80	2.04	-2.8176
DDO154	-13.007	-0.066	0.07	-0.187	0.222	-0.298	0.377	4.04	20%	-3.0437
DDO161	-11.576	-0.438	0.641	-0.996	1.505	-1.401	2.143	7.50	2.25	-2.775
DDO168	-12.993	-0.146	0.168	-0.388	0.592	-0.577	1.157	4.25	0.21	-3.0217
DDO170	-13.615	-0.245	0.288	-0.657	1.086	-0.985	1.794	15.40	4.62	-2.4626
ESO079-G014	-12.785	-0.242	0.284	-0.654	1.137	-1.008	1.776	28.70	7.17	-2.1922
ESO116-G012	-12.479	-0.273	0.362	-0.651	1.706	-0.945	2.37	13.00	3.90	-2.5361
ESO444-G084	-12.322	-0.308	0.37	-0.807	1.457	-1.153	2.589	4.83	0.48	-2.9661
ESO563-G021	-12.866	-0.088	0.094	-0.253	0.301	-0.404	0.535	60.8	9.10	-1.8662
F565-V2	-12.742	-0.258	0.306	-0.687	1.149	-1.011	2.185	51.8	10.00	-1.9357
F568-3	-13.065	-0.381	0.468	-1.09	2.097	-2.011	3.371	82.40	8.24	-1.7341
F568-V1	-12.544	-0.352	0.441	-1.056	2.656	-1.503	4.102	80.60	8.06	-1.7437
F571-8	-11.482	-0.22	0.281	-0.557	1.596	-0.783	2.307	53.30	10.70	-1.9233
F571-V1	-13.074	-0.531	0.674	-1.317	4.444	-6.797	6.756	80.10	8.00	-1.7464
F574-1	-13.03	-0.196	0.22	-0.572	0.841	-0.975	1.564	96.80	9.68	-1.6642
F583-1	-12.998	-0.254	0.293	-0.763	1.384	-1.067	2.574	35.40	8.85	-2.1011
F583-4	-13.091	-0.321	0.364	-0.937	1.353	-1.806	2.401	53.30	10.70	-1.9233
IC2574	-13.099	-0.067	0.08	-0.177	0.32	-0.26	0.56	3.91	0.20	-3.0579
IC4202	-12.607	-0.452	2.562	-0.612	4.467	-1.012	4.686	100.40	10.00	-1.6483
KK98-251	-13.834	-0.376	0.395	-5.703	1.539	-2.491	3.983	6.80	2.04	-2.8176
NGC0024	-12.862	-0.095	0.097	-0.277	0.297	-0.459	0.515	7.30	0.36	-2.7868
NGC0055	-13.205	-0.067	0.069	-0.201	0.212	-0.332	0.372	2.11	0.11	-3.3258
NGC0100	-12.603	-0.282	0.368	-0.702	1.706	-1.027	2.507	13.50	4.05	-2.5197
NGC0247	-13.451	-0.135	0.126	-0.448	0.356	-0.815	0.56	3.70	0.19	-3.0819
NGC0289	-13.489	-0.165	0.17	-0.49	0.535	-0.773	0.891	20.80	5.20	-2.332
NGC0300	-12.493	-0.351	0.47	-0.8	2.343	-1.057	3.43	2.08	0.10	-3.332
NGC0801	-13.546	-0.059	0.061	-0.175	0.191	-0.283	0.342	80.70	8.07	-1.7432
NGC0891	-12.612	-0.051	0.052	-0.148	0.16	-0.243	0.281	9.91	0.50	-2.654
NGC1003	-10.827	-0.516	0.661	-1.291	1.168	-1.726	1.47	11.40	3.42	-2.5932
NGC1090	-13.181	-0.14	0.151	-0.4	0.491	-0.629	0.784	37.00	9.25	-2.0819
NGC2403	-12.006	-0.09	0.095	-0.256	0.305	-0.368	0.462	3.16	0.16	-3.1504

TABLE I: Continued

Galaxy	A_0 best	$1\sigma_-$	$1\sigma_+$	$3\sigma_-$	$3\sigma_+$	$5\sigma_-$	$5\sigma_+$	D	D_{Error}	Z
NGC2683	-13.241	-0.096	0.096	-0.287	0.295	-0.489	0.496	9.81	0.49	-2.6584
NGC2841	-12.898	-0.055	0.058	-0.156	0.188	-0.245	0.324	14.10	1.40	-2.5009
NGC2903	-12.317	-0.104	0.106	-0.304	0.317	-0.437	0.462	6.60	1.98	-2.8305
NGC2915	-12.399	-0.104	0.113	-0.296	0.369	-0.475	0.703	4.06	0.20	-3.0415
NGC2955	-12.903	-0.134	0.139	-0.39	0.433	-0.633	0.727	97.9	9.80	-1.6593
NGC2976	-18.324	-2.469	1.421	-3.109	3.518	-3.109	4.828	3.58	0.18	-3.0962
NGC2998	-13.369	-0.1	0.105	-0.29	0.338	-0.471	0.613	68.1	10.2	-1.8169
NGC3109	-12.76	-0.075	0.084	-0.206	0.285	-0.318	0.529	1.33	0.07	-3.5262
NGC3198	-12.92	-0.094	0.101	-0.264	0.334	-0.392	0.511	13.8	1.40	-2.5102
NGC3521	-12.928	-0.115	0.119	-0.332	0.371	-0.529	0.604	7.70	2.30	-2.7636
NGC3726	-13.133	-0.149	0.159	-0.428	0.526	-0.682	0.984	18.00	2.50	-2.3948
NGC3741	-12.828	-0.07	0.076	-0.2	0.246	-0.31	0.441	3.21	0.17	-3.1436
NGC3769	-12.98	-0.141	0.153	-0.402	0.519	-0.626	1.052	18.00	2.50	-2.3948
NGC3877	-13.184	-0.745	0.577	-6.789	0.834	-6.789	1.545	18.00	2.50	-2.3948
NGC3893	-12.737	-0.139	0.148	-0.402	0.486	-0.639	0.908	18.00	2.50	-2.3948
NGC3917	-13.232	-0.184	0.186	-0.559	0.581	-0.973	1.076	18.00	2.50	-2.3948
NGC3949	-12.935	-0.32	0.292	-6.868	0.889	-7.053	1.382	18.00	2.50	-2.3948
NGC3953	-13.77	-3.868	0.454	-6.15	0.806	-6.15	1.581	18.00	2.50	-2.3948
NGC3972	-12.766	-0.19	0.19	-0.6	0.608	-1.073	1.077	18.00	2.50	-2.3948
NGC3992	-13.299	-0.099	0.102	-0.29	0.318	-0.479	0.568	23.70	2.30	-2.2753
NGC4010	-12.84	-0.168	0.175	-0.501	0.58	-0.839	1.128	18.00	2.50	-2.3948
NGC4013	-12.858	-0.083	0.089	-0.233	0.29	-0.365	0.521	18.00	2.50	-2.3948
NGC4051	-13.571	-5.087	0.431	-6.366	0.933	-6.366	1.766	18.00	2.50	-2.3948
NGC4068	-13.607	-0.335	0.331	-5.465	1.17	-6.357	1.93	4.37	0.22	-3.0096
NGC4085	-12.829	-0.212	0.212	-0.682	0.682	-1.417	1.396	18.00	2.50	-2.3948
NGC4088	-13.149	-0.147	0.155	-0.426	0.512	-0.707	0.953	18.00	2.50	-2.3948
NGC4100	-13.182	-0.094	0.099	-0.273	0.315	-0.445	0.573	18.00	2.50	-2.3948
NGC4138	-13.069	-0.213	0.212	-0.686	0.657	-1.623	1.21	18.00	2.50	-2.3948
NGC4157	-12.978	-0.121	0.13	-0.343	0.433	-0.543	0.779	18.00	2.50	-2.3948
NGC4183	-13.506	-0.145	0.151	-0.425	0.485	-0.704	0.89	18.00	2.50	-2.3948
NGC4217	-12.419	-0.181	0.208	-0.496	0.815	-0.745	1.504	18.00	2.50	-2.3948
NGC4559	-12.954	-0.258	0.318	-0.689	1.42	-0.96	2.025	9.00	2.70	-2.6958
NGC5005	-12.783	-0.28	0.246	-6.503	0.704	-7.205	1.001	16.90	1.50	-2.4222
NGC5033	-12.933	-0.1	0.101	-0.295	0.307	-0.442	0.47	15.70	4.70	-2.4542
NGC5055	-12.821	-0.098	0.098	-0.29	0.293	-0.426	0.444	9.90	0.30	-2.6544
NGC5371	-13.769	-0.09	0.092	-0.265	0.283	-0.447	0.437	39.70	9.92	-2.0513
NGC5585	-12.21	-0.37	0.552	-0.764	1.895	-1.156	2.194	7.06	2.12	-2.8013
NGC5907	-13.373	-0.04	0.041	-0.117	0.125	-0.186	0.211	17.30	0.90	-2.412
NGC5985	-13.567	-0.095	0.098	-0.28	0.31	-0.467	0.556	39.70	9.90	-2.0513
NGC6015	-13.536	-0.094	0.098	-0.272	0.306	-0.443	0.498	17.00	5.10	-2.4196
NGC6195	-13.133	-0.105	0.108	-0.312	0.329	-0.501	0.562	127.80	12.80	-1.5435
NGC6503	-12.827	-0.043	0.045	-0.126	0.142	-0.201	0.239	6.26	0.31	-2.8535
NGC6674	-13.504	-0.082	0.085	-0.238	0.264	-0.39	0.452	51.20	10.20	-1.9408
NGC6789	-12.214	-0.284	0.314	-0.841	1.141	-1.492	2.393	3.52	0.18	-3.1035
NGC6946	-13.033	-0.098	0.099	-0.293	0.3	-0.466	0.462	5.52	1.66	-2.9081
NGC7331	-12.785	-0.063	0.066	-0.18	0.211	-0.275	0.353	14.70	1.50	-2.4828
NGC7793	-13.243	-0.205	0.23	-0.57	0.823	-0.926	1.676	3.61	0.18	-3.0926
NGC7814	-12.572	-0.058	0.058	-0.18	0.171	-0.307	0.284	14.40	0.66	-2.4917
UGC00128	-13.691	-0.116	0.128	-0.32	0.429	-0.487	0.735	64.50	9.70	-1.8405
UGC00191	-13.65	-0.241	0.259	-0.707	0.887	-1.159	1.378	17.10	5.10	-2.4171
UGC00634	-12.969	-0.379	0.45	-1.014	1.701	-1.469	2.544	30.90	7.70	-2.1601
UGC00731	-13.257	-0.32	0.369	-0.98	1.834	-2.166	2.757	12.50	3.75	-2.5532
UGC00891	-12.334	-0.379	0.554	-0.8	2.19	-1.214	2.594	10.20	3.10	-2.6415
UGC01281	-12.981	-0.083	0.08	-0.263	0.233	-0.476	0.384	5.27	0.24	-2.9283
UGC02259	-13.736	-0.236	0.251	-0.705	0.85	-1.283	1.635	10.50	3.10	-2.6289
UGC02487	-13.349	-0.074	0.075	-0.22	0.229	-0.357	0.377	69.10	10.40	-1.8106
UGC02885	-12.964	-0.101	0.105	-0.292	0.33	-0.463	0.577	80.60	8.06	-1.7437
UGC02916	-13.551	-0.156	0.153	-0.515	0.465	-1.21	0.758	65.40	9.80	-1.8345
UGC02953	-13.032	-0.067	0.069	-0.2	0.211	-0.281	0.338	16.50	4.95	-2.4326
UGC03205	-13.201	-0.085	0.088	-0.245	0.275	-0.39	0.461	50.00	10.00	-1.9511
UGC03546	-12.884	-0.103	0.107	-0.313	0.352	-0.453	0.639	28.70	7.20	-2.1922
UGC03580	-10.529	-0.525	0.646	-1.473	1.102	-2.141	1.434	20.70	5.20	-2.3341

TABLE I: Continued

Galaxy	A_0 best	$1\sigma_-$	$1\sigma_+$	$3\sigma_-$	$3\sigma_+$	$5\sigma_-$	$5\sigma_+$	D	D_{Error}	Z
UGC04278	-12.504	-0.319	0.426	-0.766	2.138	-1.135	2.641	9.51	2.85	-2.6719
UGC04325	-13.656	-5.926	0.625	-6.163	1.357	-6.163	3.269	9.60	2.88	-2.6678
UGC04483	-13.395	-0.141	0.142	-0.428	0.434	-0.733	0.759	3.34	0.31	-3.1263
UGC04499	-13.231	-0.297	0.344	-0.872	1.609	-1.371	3.036	12.50	3.75	-2.5532
UGC05005	-13.197	-0.419	0.501	-1.185	2.231	-1.859	4.122	53.70	10.70	-1.9201
UGC05253	-12.707	-0.085	0.086	-0.255	0.259	-0.398	0.411	22.90	5.72	-2.2902
UGC05414	-13.154	-0.322	0.371	-1.043	1.974	-2.442	2.8	9.40	2.82	-2.6769
UGC05716	-13.273	-0.285	0.343	-0.732	1.225	-1.11	1.652	21.30	5.30	-2.3217
UGC05721	-12.573	-0.241	0.291	-0.641	1.266	-0.906	2.059	6.18	1.85	-2.8591
UGC05750	-13.355	-0.285	0.313	-0.861	1.124	-2.09	2.168	58.70	11.70	-1.8814
UGC05764	-14.603	-1.104	2.539	-1.545	4.629	-1.545	5.561	7.47	2.24	-2.7768
UGC05829	-13.033	-0.602	0.717	-2.34	4.449	-6.898	5.976	8.64	2.59	-2.7136
UGC05918	-13.083	-0.334	0.38	-0.979	1.702	-1.592	2.999	7.66	2.30	-2.7658
UGC05986	-12.436	-0.24	0.306	-0.605	1.531	-0.851	2.004	8.63	2.59	-2.7141
UGC06399	-12.847	-0.167	0.172	-0.51	0.562	-0.906	1.109	18.00	2.50	-2.3948
UGC06446	-13.18	-0.266	0.301	-0.76	1.177	-1.187	1.956	12.00	3.60	-2.5709
UGC06614	-12.415	-0.372	0.479	-0.968	2.554	-1.336	4.065	88.70	8.87	-1.7022
UGC06667	-12.561	-0.136	0.149	-0.388	0.516	-0.608	1.042	18.00	2.50	-2.3948
UGC06786	-12.087	-0.158	0.178	-0.418	0.606	-0.597	0.909	29.30	7.32	-2.1832
UGC06787	-13.387	-0.048	0.05	-0.139	0.156	-0.218	0.277	21.30	5.32	-2.3217
UGC06818	-13.089	-0.18	0.184	-0.549	0.595	-0.935	1.175	18.00	2.50	-2.3948
UGC06917	-12.882	-0.166	0.172	-0.491	0.567	-0.819	1.112	18.00	2.50	-2.3948
UGC06923	-13.031	-0.196	0.195	-0.63	0.622	-1.401	1.232	18.00	2.50	-2.3948
UGC06930	-13.382	-0.356	0.37	-1.354	1.399	-4.689	3.052	18.00	2.50	-2.3948
UGC06983	-13.01	-0.149	0.158	-0.432	0.524	-0.7	1.021	18.00	2.50	-2.3948
UGC07089	-13.308	-0.189	0.189	-0.604	0.609	-1.175	1.143	18.00	2.50	-2.3948
UGC07125	-13.871	-0.285	0.327	-0.877	1.551	-1.516	2.282	19.80	5.90	-2.3534
UGC07151	-13.265	-0.131	0.12	-0.437	0.337	-0.837	0.524	6.87	0.34	-2.8131
UGC07232	-12.847	-0.213	0.203	-0.726	0.611	-3.71	1.102	2.83	0.17	-3.1983
UGC07261	-13.236	-0.719	0.839	-6.698	3.382	-6.698	6.573	13.10	3.93	-2.5328
UGC07323	-13.118	-0.383	0.407	-2.974	2.245	-6.843	2.622	8.00	2.40	-2.747
UGC07399	-12.272	-0.252	0.308	-0.676	1.453	-0.957	2.208	8.43	2.53	-2.7242
UGC07524	-13.326	-0.142	0.143	-0.436	0.438	-0.765	0.751	4.74	0.24	-2.9743
UGC07559	-13.614	-0.167	0.155	-0.572	0.444	-1.645	0.79	4.97	0.25	-2.9537
UGC07577	-14.597	-3.045	0.474	-5.333	0.813	-5.333	1.459	2.59	0.13	-3.2368
UGC07603	-12.501	-0.266	0.346	-0.659	1.715	-0.943	2.149	4.70	1.41	-2.978
UGC07690	-13.541	-0.389	0.404	-6.31	1.609	-6.454	2.388	8.11	2.43	-2.7411
UGC07866	-13.476	-0.269	0.265	-0.935	0.861	-6.501	1.448	4.57	0.23	-2.9902
UGC08286	-12.989	-0.061	0.06	-0.189	0.176	-0.323	0.29	6.50	0.21	-2.8372
UGC08490	-12.963	-0.119	0.128	-0.34	0.413	-0.54	0.735	4.65	0.53	-2.9826
UGC08550	-12.975	-0.241	0.302	-0.622	1.329	-0.885	2.039	6.70	2.00	-2.824
UGC08699	-12.978	-0.122	0.137	-0.34	0.479	-0.521	0.861	39.30	9.82	-2.0557
UGC08837	-13.599	-0.129	0.12	-0.439	0.35	-0.909	0.588	7.21	0.36	-2.7921
UGC09037	-12.876	-0.136	0.146	-0.382	0.478	-0.588	0.839	83.6	8.40	-1.7279
UGC09133	-13.146	-0.065	0.065	-0.192	0.197	-0.318	0.297	57.10	11.40	-1.8934
UGC09992	-13.996	-5.379	0.911	-5.672	3.04	-5.672	7.389	10.70	3.21	-2.6207
UGC10310	-13.29	-0.772	0.746	-6.666	1.808	-6.666	4.33	15.20	4.60	-2.4682
UGC11455	-12.841	-0.095	0.103	-0.268	0.337	-0.416	0.58	78.60	11.80	-1.7547
UGC11557	-13.209	-1.105	1.227	-6.676	4.01	-6.676	6.456	24.20	6.05	-2.2663
UGC11820	-13.069	-0.379	0.47	-0.938	1.757	-1.34	2.426	18.10	5.43	-2.3924
UGC11914	-12.274	-0.128	0.129	-0.38	0.384	-0.61	0.575	16.90	5.10	-2.4222
UGC12506	-13.546	-0.116	0.117	-0.355	0.359	-0.624	0.625	100.60	10.10	-1.6475
UGC12632	-13.674	-0.35	0.361	-2.922	1.682	-6.297	2.197	9.77	2.93	-2.6602
UGC12732	-13.386	-0.356	0.399	-1.003	1.481	-1.743	2.227	13.20	4.00	-2.5295
UGCA442	-12.786	-0.133	0.165	-0.329	0.629	-0.462	1.305	4.35	0.22	-3.0116
UGCA444	-13.26	-0.077	0.078	-0.231	0.242	-0.381	0.415	0.98	0.05	-3.6588